THE JOURNAL OF PHYSICAL CHEMISTRY B

Article

pubs.acs.org/JPCB

Nonlinear THz Conductivity Dynamics in P-Type CVD-Grown Graphene

Harold Y. Hwang,[†] Nathaniel C. Brandt,[†] Hootan Farhat,[‡] Allen L. Hsu,[‡] Jing Kong,[‡] and Keith A. Nelson*[,†]

[†]Department of Chemistry, Massachusetts Institute of Technology, Cambridge, Massachusetts, United States

[‡]Research Laboratory of Electronics, Massachusetts Institute of Technology, Cambridge, Massachusetts, United States

ABSTRACT: We report strong THz-induced transparency in CVD-grown graphene where 92−96% of the peak-field is transmitted compared to 74% at lower field strength. Time-resolved THz pump/THz probe studies reveal that the absorption recovers in 2−3 ps. The induced transparency is believed to arise from nonlinear pumping of carriers in graphene which suppresses the mobility and consequently the conductivity in a spectral region where the light−matter interaction is particularly strong.

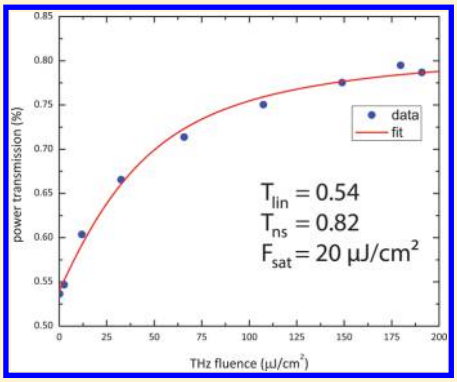

The discovery of single-layer graphene has generated intense fundamental scientific and technological interest over the past several years. The characteristic linear electronic dispersion of the material gives rise to massless Dirac fermions which have a constant Fermi velocity.[1] As a result, graphene exhibits unique carrier transport properties that are of interest in electronics and optics applications. Recent advances in large-area graphene fabrication by chemical vapor deposition[2] have shown promise for the development of practical graphene electronic and optical devices.[3,4] As a result, exploring fundamental properties of such samples is of paramount importance.

The dc to THz frequency conductivity of doped graphene can be large compared to the conductivity at higher frequencies (mid-IR to visible).[5,6] In the intrinsic doping limit, several theoretical investigations have predicted extraordinary effects from both electronic and electromagnetic stimuli, including nonlinear frequency conversion and nonlinear conductivity effects due to the strong interaction of low-frequency light with graphene.[7−12] Ultrafast studies of photoexcited carriers in graphene with visible to near-IR pumping and visible to THz probing have revealed various aspects of inter- and intraband conductivity dynamics.[5,13−15] Excitation of doped graphene in the visible to near-IR range is weak compared to THz excitation which is enhanced due to excess free carrier absorption.[6] Furthermore, the creation of electron−hole pairs in graphene with optical excitation leads to complicated relaxation dynamics related to electron−hole recombination. Other recent demonstrations have shown strong nonlinear spectroscopic responses in graphene pumped with light in the THz to mid-IR range.[16−18]

Tabletop generation of THz pulses with microjoule energies and field amplitudes of hundreds of kV/cm[19] has enabled nonlinear electronic spectroscopy of conventional semiconductors,[20−22] revealing carrier mobility saturation and impact ionization dynamics due to accelerated carriers. Such demonstrations have shown that semiconductors can be suitable for applications like ultrafast THz saturable absorbers.[23] Recent theoretical and experimental work has also demonstrated that graphene is a good saturable absorber in the near-IR to visible range.[3,4] Here we present nonlinear THz transmission results that demonstrate THz-induced transparency in room-temperature graphene, and we study the dynamics of the nonlinear response with time-resolved THz pump/THz probe measurements.

High-field THz pulses were generated by optical rectification with tilted pulse front (TPF) excitation in lithium niobate (LN), giving pulse energies in excess of 3 μJ at 1 kHz repetition rate.[19,24,25] THz pulses were collimated and focused onto the sample with a pair of off-axis parabolic mirrors, and the transmitted THz light was imaged onto a ZnTe electro-optic sampling crystal for detection. The maximum THz energy at the sample was 1.5 μJ and the spot size was 1 mm, giving a maximum fluence of 190 μJ/cm^2. THz fluence-dependent transmission measurements were performed by varying the THz pulse transmission through a pair of polarizers prior to the sample, as shown in Figure 1. The time-dependent THz field

Special Issue: Michael D. Fayer Festschrift

Received: July 29, 2013
Revised: October 8, 2013
Published: October 8, 2013

ACS Publications © 2013 American Chemical Society

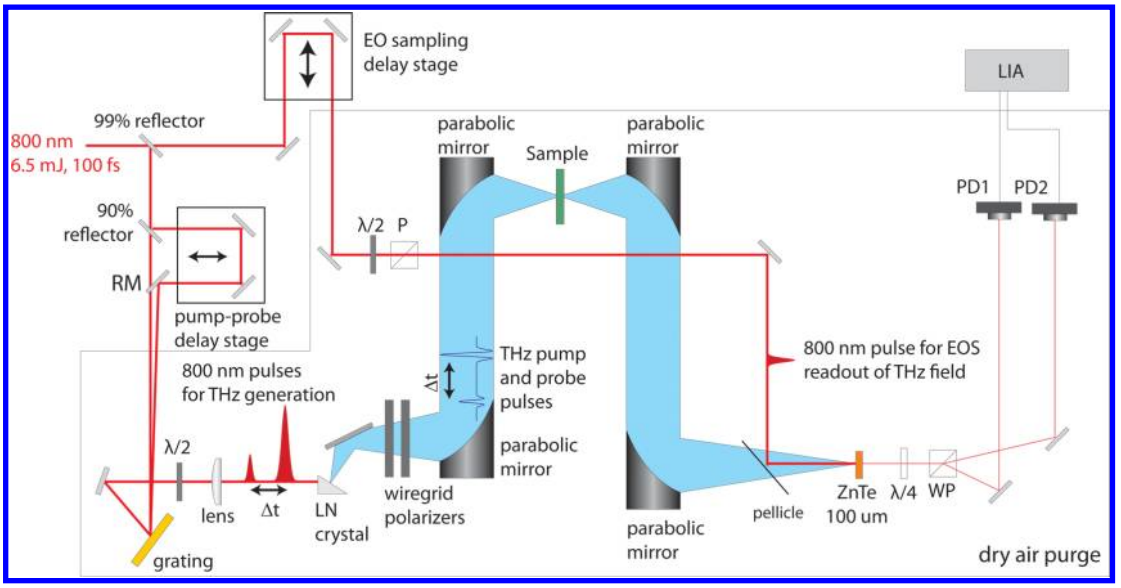

Figure 1. Nonlinear THz transmission and THz pump/THz probe setup. The output of an amplified laser system is split into two arms with a 99% beam splitter. The 99% reflection is used to generate high-field THz pulses, while the 1% transmitted arm is used for electro-optic detection of the THz electric field. A pair of wiregrid polarizers is used to variably attenuate the THz pulses in order to measure field-dependent effects. For THz pump/THz probe measurements, the 800 nm THz generation pulse is split into pump and probe arms that generate the THz pump and THz probe pulses, respectively. An optical stage delays the pump with respect to the probe, yielding variably time-delayed THz pulses from a common lithium niobate generation crystal. RM, recombination mirror; EO/EOS, electro-optic sampling; LN, lithium niobate; $\lambda/2$, half-waveplate; $\lambda/4$, quarter-waveplate; WP, Wollaston prism; PD, photodiode; LIA, lock-in amplifier.

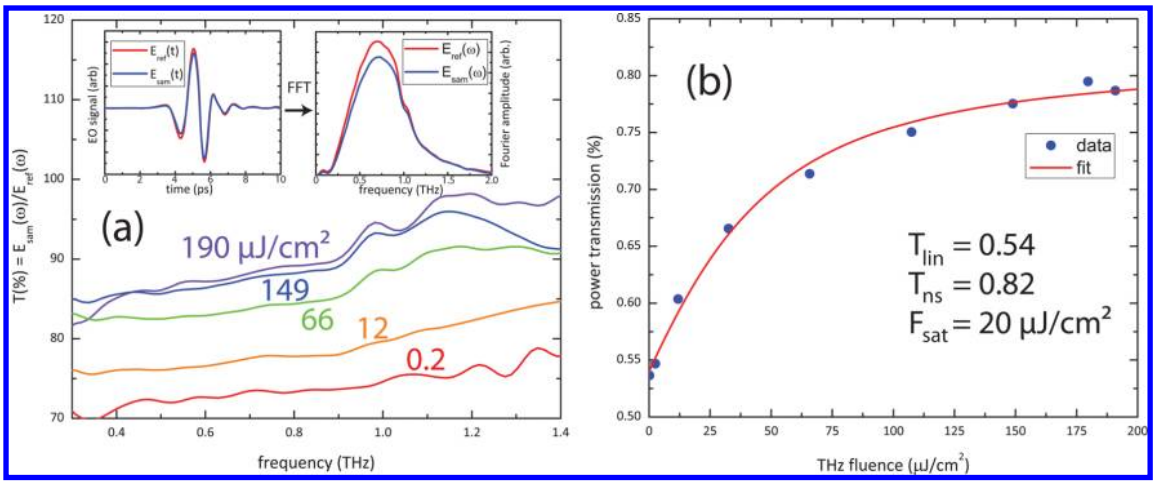

Figure 2. (a) THz field percent transmission spectra of CVD graphene on fused silica at different fluences. The transmission increases as the THz field strength increases. (b) THz power transmission integrated over the entire THz pulse versus THz fluence. The fit is to a saturable transmission function (eq 1).

profile after passing through the sample $E_{sam}(t)$ (graphene on substrate) or with the bare substrate $E_{ref}(t)$ was measured by electro-optic sampling with a variably delayed 800 nm readout pulse.[26,27] Fourier transformation of the field profiles yielded the THz spectra $E_{sam}(\omega)$ and $E_{ref}(\omega)$.

THz pump/THz probe measurements were performed in a collinear geometry by splitting the optical pulse used for THz generation into pump and probe pulses with an adjustable time delay between them and then recombining them in a common LN crystal[20−22] (Figure 1), resulting in collinear and copolarized time-delayed THz pulses of approximately the same spot size at the sample. For the time-resolved measurements, the peak amplitude in the transmitted THz probe field profile is reported as a function of THz pump−probe delay. The ratio of the pump and probe field strengths is about 20:1, minimizing the effect of the probe on the sample. Comparison of the average power transmission with the peak-field transmission (both discussed below) showed reasonable agreement, indicating that the peak transmission could be used to report changes in the overall transmission of the sample. Full time- and frequency-resolved THz pump−probe measurements, where the full probe field was resolved for each pump−probe delay time, revealed no detectable phase shift in the THz probe electric field, suggesting that the transmission of the peak amplitude of the probe field is a suitable metric for observing changes in the graphene conductivity response.

Graphene samples were grown on a copper substrate by chemical vapor deposition[2] and transferred to either 1.4 mm thick fused silica or 1 mm thick high resistivity silicon substrates. The graphene covered roughly half of the substrate

dx.doi.org/10.1021/jp407548a | J. Phys. Chem. B 2013, 117, 15819−15824

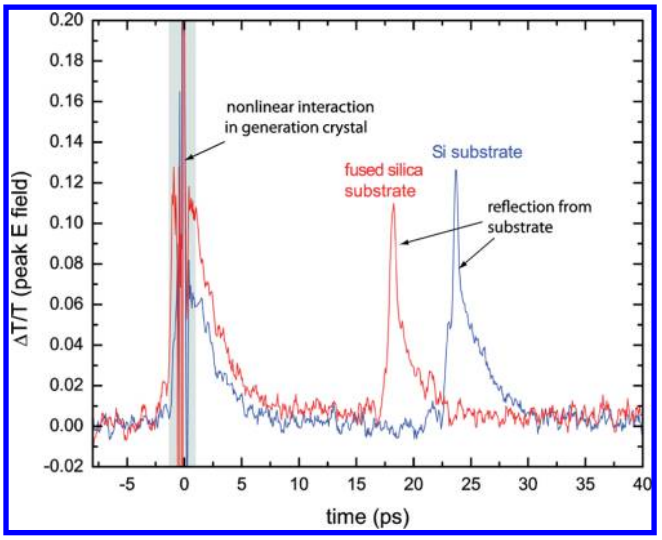

Figure 3. THz pump/THz probe peak field scans for graphene on fused silica (red) and silicon (blue). The EOS delay was set so that the optical readout pulse was temporally overlapped with the peak of the transmitted THz probe pulse, and the THz pump−probe time interval was varied. The large signals at time zero may have contributions from the nonlinear interaction of the optical pump pulses that were temporally overlapped in the THz generation crystal. The second signals are due to reflections of the THz pump pulse in the sample substrates; the time delays are consistent with the THz refractive indices in fused silica and silicon. The second signals are reproduced in Figure 4.

area, which allowed us to record reference and sample scans with a common substrate. Hall effect measurements on several device sizes indicated a sheet hole concentration of about 5.5×10^{12} cm^{-2} for either fused silica or silicon substrate samples. On the basis of a linear density of states and a Fermi−Dirac thermal distribution, the Fermi energy was calculated to be $E_f \approx -270$ meV for both samples.[28] Atomic force microscopy and Raman spectroscopy[29] of the sample revealed that it was predominantly single-layer graphene.

Figure 2a shows the spectrally resolved THz field transmission $T = |E_{sam}(\omega)|/|E_{ref}(\omega)|$ for various THz field strengths as a function of frequency, indicating induced transparency whose extent increases with increasing fluence. This can be attributed to a decrease in carrier mobility as THz excitation redistributes carrier energies within the conduction band.[7,8] In this case, the largest effect comes from redistribution of holes, since the sample is strongly hole-doped.

The inset of Figure 2a shows representative THz time and frequency profiles measured in the experiment. Figure 2b shows the power transmission of the entire THz pulse, $\int E_{sam}^2(t)\,dt/\int E_{ref}^2(t)\,dt$, plotted versus THz fluence. The average power transmission went from 54% at low fluence to 79% at the highest THz fluence (corresponding to 73 and 89% average field transmission). The corresponding peak field transmission ($\max(E_{sam})/\max(E_{ref})$) went from 74 to 87%, which agrees within experimental uncertainties (estimated at 2−3%) with the average field transmission values above. The power transmission was fit to a saturable power transmission function:[23]

$$T(F_p) = T_{ns}\frac{\ln\left[1 + \frac{T_{lin}}{T_{ns}}(e^{F_p/F_{sat}} - 1)\right]}{F_p/F_{sat}} \quad (1)$$

where T_{lin} and T_{ns} are the limiting linear and nonsaturable power transmission coefficients, F_p is the THz fluence, and F_{sat} is the saturation fluence. From our fit, we found $T_{lin} = 0.54$, $T_{ns} = 0.82$, and $F_{sat} = 20\ \mu J/cm^2$.

At first glance, the strong induced transparency that we measure is in contrast to expectations from simple heating in a Drude-like treatment of the frequency-dependent intraband conductivity σ in graphene:[5,13−15]

$$\frac{\sigma_{intra}(\omega)}{\sigma_Q} = \frac{8k_BT}{\pi\hbar}\ln(e^{-E_F/2k_BT} + e^{E_F/2k_BT})\frac{1}{\omega^2\tau + 1/\tau} \quad (2)$$

where σ_Q is the universal dc quantum conductivity, T is the temperature, E_F is the Fermi energy, and τ is the momentum scattering time. Here the electron and hole responses are symmetric, such that electron- or hole-doped graphene should exhibit the same conductivity. Hole-doped graphene at our carrier sheet densities should only exhibit an intraband response, since the calculated Fermi energy far exceeds the photon energies of our THz pulses. As a result, we ignore the

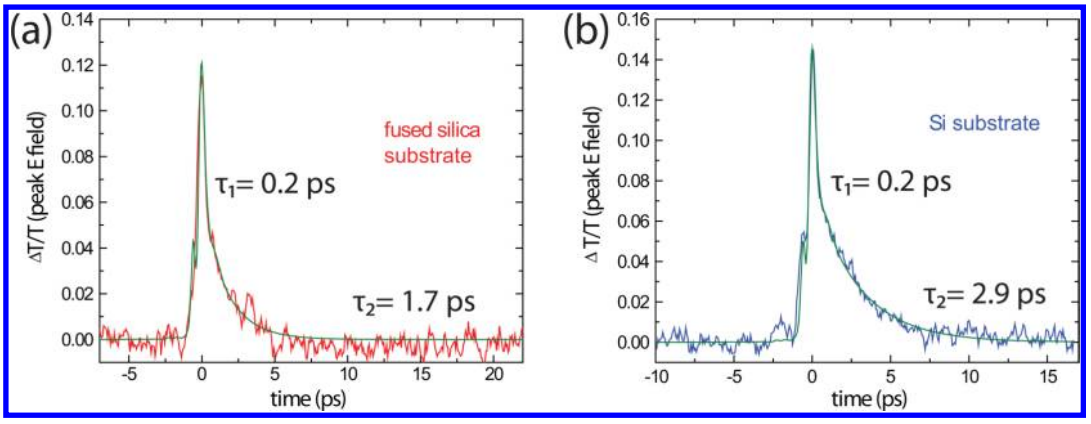

Figure 4. THz pump/THz probe data from graphene on fused silica and silicon substrates. The zero of time corresponds to the arrival of the THz pulse in the graphene after an internal reflection at the substrate−air interface. The data were fit to a convolution of the square of the THz pump field with a biexponential decay. The fast components of the fits labeled τ_1 are shorter than the instrumental time resolution given by the THz field profile. The slower components are consistent with those of the responses observed following the initial signals shown in Figure 3 as well as the signals following an additional round-trip of the THz pump pulse in the substrates.

dx.doi.org/10.1021/jp407548a | J. Phys. Chem. B 2013, 117, 15819−15824

interband contribution to the conductivity. The conductivity can be related to the transmission T by

$$T(\omega) = \frac{1}{\left|1 + \frac{Z_0\sigma(\omega)}{n_s + 1}\right|^2} \quad (3)$$

where Z_0 is the vacuum impedance and n_s is the substrate refractive index.

Under this treatment, it is assumed that the pump pulse creates a distribution of hot carriers that thermalize among themselves in a short time compared to the experimental time resolution (~100 fs). Assuming that the THz pulse only heats the carrier distribution, the transmission spectra should show a decrease in transmission (i.e., increased absorption) based on eq 2 for the intraband conductivity (assuming a hot distribution of carriers would exhibit the same momentum relaxation time). However, our experiments show a strong induced transparency and not induced absorption.

Theoretical treatments of graphene under a dc bias or ac excitation at THz frequencies[7,8] have predicted a very strong decrease in carrier mobility and consequently a decrease in conductivity at even modest field strengths (~1 kV/cm). These studies take into account damping due to electron-impurity, electron-acoustic phonon, and electron-optic phonon scattering at typical carrier densities (N = (0.5−1.5) × 10^{12} cm^{-2}). By separating the mobility into impurity, acoustic phonon, and optic phonon contributions at various lattice temperatures, it is possible to assess which scattering mechanisms dominate in the conductivity. At low lattice temperatures, impurity scattering dominates. At moderate temperatures (T ~ 300 K), acoustic phonon scattering becomes significant, and finally at still higher temperatures (T > 700 K) optic phonon scattering becomes significant. For the nonlinear conductivity response, similar arguments explain the decrease in conductivity with increasing field strength, since the relative change in electron temperature versus lattice temperature decreases with increasing lattice temperature. Rapid partial thermalization of the hot carriers with the lattice within the THz pulse duration of ~1 ps increases the lattice temperature, and the resulting increased phonon population results in faster electron−phonon scattering and decreased carrier mobility.

Indeed, increasing the momentum scattering rate in the Drude-like conductivity (eq 2) leads to induced transparency in the transmission (noting that the Drude-like conductivity is a relatively weak function of temperature and Fermi level). Taking a simplified approach to understanding the phenomenology of THz saturable absorption in graphene in terms of a Drude-like treatment of the conductivity, we fit the power transmission (Figure 2b) to eq 2, giving τ = 45 fs at the lowest fluence and τ = 18 fs at the highest fluence. This indicates a large increase in the momentum scattering rate, which leads to decreased carrier mobility, with increasing pump fluence.

Though empirically similar, it is worth noting that THz-induced transparency in graphene is quite different from that in conventional semiconductors. In conventional semiconductors, the mobility is determined by the average effective mass in a given part of the conduction band, where heating a distribution of electrons leads to inter- and intravalley scattering into lower mobility regions of the conduction band. This is different in the case of graphene, where the linear dispersion implies zero effective mass for a large range of energies, and therefore hotter distributions of electrons or holes do not experience different effective masses. Furthermore, there is symmetry between holes and electrons in graphene arising from the symmetric linear electronic dispersion. At high THz pump fluences, the interactions giving rise to the reduced mobility occur through scattering processes from impurities and phonons as discussed above. In conventional semiconductors, the scattering processes are thought to mainly contribute to the relaxation of energetic carriers after excitation.

Since the mobility of the graphene layer is affected by the THz excitation pulse through enhanced scattering, the formation of the nonequilibirum distribution of carriers likely plays a strong role in THz saturable absorption. Auger recombination and impact ionization in the graphene layer provide mechanisms for changing the carrier densities.[16,18,30,31] Impact ionization dominates over Auger recombination after THz excitation of the system, leading to higher carrier densities and a nonequilibrium carrier distribution.[16,32] The non-equilibrium carrier distribution thermalizes faster than the THz excitiation pulse duration, and on longer time scales thermalizes with the lattice via optic phonon emission.

Time-resolved THz pump/THz probe measurements were performed in a collinear geometry, as has been described in previous work[20−22] by directing two variably delayed optical pulses into the lithium niobate nonlinear crystal to generate a strong THz pump pulse and a weak THz probe pulse. The signal at t = 0 was not reliable because this corresponded to the two optical pulses that generated the THz pump and probe pulses overlapping temporally inside the LN crystal where they could interact nonlinearly, influencing the THz generation process. However, there was a significant back-reflection of the THz pump pulse from the substrate−air interface (~35 and 55% reflection of the THz field per interface in fused silica and silicon, respectively), and the reflected THz pump pulse, upon its return to the graphene layer, was sufficiently intense to produce a significant change in probe pulse transmission. The signal from each sample, shown in Figure 3, therefore consists of two temporally separated components: a signal that starts at t = 0, which is only reliable at time delays greater than the THz pulse duration of about 1 ps, and another signal that starts when the THz pump−probe delay time matches the THz round-trip time t_{RT} (roughly 20 ps) in the substrate. Since the second signal component permits reliable measurement of the sample response at short probe delay times relative to t_{RT}, we used this component for our analysis. In principle, the signal could be influenced by sample responses from the first pass of the THz pump pulse through the graphene layer at t = 0 as well as the second pass at $t = t_{RT}$, but the sample response does not appear to persist for nearly that long. The time-dependent data shown in Figure 4 are the second signals in Figure 3, with the time axes rescaled to set t = 0 as the arrival time of the reflected THz pump pulse. Although the signals at around 20 and 40 ps (not shown) are smaller than those at time zero due to the Fresnel losses at each interface for each round trip of the pump in the substrate, the dynamics of the sample responses appear to be the same. Although we cannot analyze the short-time response observed in the signal at zero delay, the slower component that follows is similar to the slower responses after one or two pump pulse round-trips. Therefore, in the fluence regime from the first to the third pump field interaction, there does not appear to be a fluence dependence in the dynamics. This seems to suggest that, though the THz pump pulse induces transparency in the sample through carrier mobility suppression mediated by increased momentum scattering rate,

the energy relaxation rate is independent of the nonequilibrium distribution of carriers.

The results shown in Figure 4 reveal partial recovery of graphene absorption with a dynamical component that is faster than the time resolution given by the duration of a single lobe of the THz pulse and a slower component that can be fit to an exponential decay with τ_r = 1.7 ps for graphene on fused silica and τ_r = 2.9 ps for graphene on silicon. The difference in carrier relaxation times may be attributed to differences in coupling of the graphene layer to the phonons of the substrate or to differences in the inhomogeneities and impurity or defect densities of the graphene samples. The peak change in $\Delta T/T$ reaches 12 and 14%, corresponding respectively to absolute transmission of the THz probe pulse of 92 and 96% (85 and 92% in peak intensity transmission), in the fused silica and silicon substrates. This is in good agreement with the maximum power transmission obtained from a fit to the saturable power transmission function (eq 1 with T_{ns} = 0.82) above.

In conclusion, we observed strong THz-induced transparency in CVD-grown graphene. We believe the effect is due to creation of electron−hole pairs and carrier redistribution by the THz pulse, which suppresses the carrier mobility through enhanced scattering processes at higher carrier densities and lattice energies. Time-resolved THz pump/THz probe spectroscopy indicated absorption recovery on a picosecond time scale, which is consistent with similar studies performed with optical pump pulses and which has been associated with electron−hole recombination as well as carrier cooling.[5,13−15] Our results suggest that graphene is suitable for use as an ultrafast THz saturable absorber. Further study is needed to fully explain the phenomena observed in our experiments including more detailed theoretical treatments of THz field interactions and the temperature-dependent scattering processes that mediate carrier mobility and relaxation.

AUTHOR INFORMATION

Corresponding Author

*E-mail: kanelson@mit.edu.

Notes

The authors declare no competing financial interest.

ACKNOWLEDGMENTS

The authors would like to acknowledge funding from ONR grants N00014-06-1-0459 and N00014-09-1-1103 and NSF grant 1111557 and Drs. Keshav Dani and Sharly Fleischer and Prof. Mildred Dresselhaus for helpful discussions.

REFERENCES

(1) Geim, A. K.; Novoselov, K. S. The Rise of Graphene. *Nat. Mater.* **2007**, *6*, 183−191.

(2) Li, X.; Cai, W.; An, J.; Kim, S.; Nah, J.; Yang, D.; Piner, R.; Velamakanni, A.; Jung, I.; Tutuc, E.; Banerjee, S. K.; Colombo, L.; Ruoff, R. S. Large-Area Synthesis of High-Quality and Uniform Graphene Films on Copper Foils. *Science* **2009**, *324*, 1312−1314.

(3) Xing, G.; Guo, H.; Zhang, X.; Sum, T. C.; Huan, C. H. A. The Physics of Ultrafast Saturable Absorption in Graphene. *Opt. Express* **2010**, *18*, 4564−4573.

(4) Bao, Q.; Zhang, H.; Wang, Y.; Ni, Z.; Yan, Y.; Shen, Z. X.; Loh, K. P.; Tang, D. Y. Atomic-Layer Graphene as a Saturable Absorber for Ultrafast Pulsed Lasers. *Adv. Funct. Mater.* **2009**, *19*, 3077−3083.

(5) Choi, H.; Borondics, F.; Siegel, D. A.; Zhou, S. Y.; Martin, M. C.; Lanzara, A.; Kaindl, R. A. Broadband Electromagnetic Response and Ultrafast Dynamics of Few-Layer Epitaxial Graphene. *Appl. Phys. Lett.* **2009**, *94*, 172102-1−172102-3.

(6) Mak, K. F.; Sfeir, M. Y.; Wu, Y.; Lui, C. H.; Misewich, J. A.; Heinz, T. F. Measurement of the Optical Conductivity of Graphene. *Phys. Rev. Lett.* **2008**, *101*, 196405-1−196405-4.

(7) Bao, W. S.; Liu, S. Y.; Lei, X. L.; Wang, C. M. Nonlinear DC Transport in Graphene. *J. Phys.: Condens. Matter* **2009**, *21*, 305302-1−305302-5.

(8) Bao, W. S.; Liu, S. Y.; Lei, X. L. Hot-Electron Transport in Graphene Driven by Intense Terahertz Fields. *Phys. Lett. A* **2010**, *374*, 1266−1269.

(9) Mikhailov, S. A. Non-linear Electromagnetic Response of Graphene. *Europhys. Lett.* **2007**, *9*, 27002-1−27002-4.

(10) Mikhailov, S. A.; Ziegler, K. Nonlinear Electromagnetic Response of Graphene: Frequency Multiplication and the Self-Consistent-Field Effects. *J. Phys.: Condens. Matter* **2008**, *20*, 384204-1−384204-10.

(11) Mikhailov, S. A. Non-linear Graphene Optics for Terahertz Applications. *Microelectron. J.* **2009**, *40*, 712−715.

(12) Wright, A. R; Xu, X. G.; Cao, J. C.; Zhang, C. Strong Nonlinear Optical Response of Graphene in the Terahertz Regime. *Appl. Phys. Lett.* **2009**, *95*, 072101-1−072101-3.

(13) Dawlaty, J. M.; Shivaraman, S.; Strait, J.; George, P.; Chandrashekhar, M.; Rana, F.; Spencer, M. G.; Veksler, D.; Chen, Y. Measurement of the Optical Absorption Spectra of Epitaxial Graphene from Terahertz to Visible. *Appl. Phys. Lett.* **2008**, *93*, 131905-1−131905-3.

(14) George, P. A.; Strait, J.; Dawlaty, J.; Shivaraman, S.; Chandrashekhar, M.; Rana, F.; Spencer, M. G. Ultrafast Optical-Pump Terahertz-Probe Spectroscopy of the Carrier Relaxation and Recombination Dynamics in Epitaxial Graphene. *Nano Lett.* **2008**, *8*, 4248−4251.

(15) Dani, K. M.; Lee, J.; Sharma, R.; Mohite, A. D.; Galande, C. M.; Ajayan, P. M.; Dattelbaum, A. M.; Htoon, H.; Taylor, A. J.; Prasankumar, R. P. Intraband conductivity response in graphene observed using ultrafast infrared-pump visible-probe spectroscopy. *Phys. Rev. B* **2012**, *86*, 125403-1−125403-7.

(16) Tani, S.; Blanchard, F.; Tanaka, K. Ultrafast Carrier Dynamics in Graphene Under a High Electric Field. *Phys. Rev. Lett.* **2012**, *109*, 166603-1−166603-5.

(17) Woerner, M.; Kuehn, W.; Bowlan, P.; Reimann, K.; Elsaesser, T. Ultrafast Two-Dimensional Terahertz Spectroscopy of Elementary Excitations in Solids. *New J. Phys.* **2013**, *15*, 025039-1−025039-16.

(18) Winnerl, S.; Orlita, M.; Plochocka, P.; Kossacki, P.; Potemski, M.; Winzer, T.; Malic, E.; Knorr, A.; Sprinkle, M.; Berger, C.; de Heer, W. A.; Schneider, H.; Helm, M. Carrier Relaxation in Epitaxial Graphene Photoexcited Near the Dirac Point. *Phys. Rev. Lett.* **2011**, *107*, 237401-1−237401-5.

(19) Yeh, K. L; Hoffmann, M. C.; Hebling, J.; Nelson, K. A. Generation of 10 mJ Ultrashort Terahertz Pulses by Optical Rectification. *Appl. Phys. Lett.* **2007**, *90*, 171121-1−171121-3.

(20) Hoffmann, M. C.; Hebling, J.; Hwang, H. Y.; Yeh, K.-L.; Nelson, K. A. THz-pump/THz-probe Spectroscopy of Semiconductors at High Field Strengths [Invited]. *J. Opt. Soc. Am. B* **2009**, *26*, A29−A34.

(21) Hoffmann, M. C.; Hebling, J.; Hwang, H. Y.; Yeh, K.-L.; Nelson, K. A. Impact Ionization in InSb Probed by Terahertz pump—Terahertz Probe Spectroscopy. *Phys. Rev. B* **2009**, *79*, 161201(R)-1−161201(R)-4.

(22) Hebling, J.; Hoffmann, M. C.; Hwang, H. Y.; Yeh, K.-L.; Nelson, K. A. Observation of Nonequilibrium Carrier Distribution in Ge, Si, and GaAs by Terahertz Pump−Terahertz Probe Measurements. *Phys. Rev. B* **2010**, *81*, 035201-1−035201-5.

(23) Hoffmann, M. C.; Turchinovich, D. Semiconductor Saturable Absorbers for Ultrafast Terahertz Signals. *Appl. Phys. Lett.* **2010**, *96*, 151110-1−151110-3.

(24) Feurer, T.; Stoyanov, N. S.; Ward, D. W.; Vaughan, J. C.; Statz, E. R.; Nelson, K. A. Terahertz Polaritonics. *Annu. Rev. Mater. Res.* **2007**, *37*, 317−350.

(25) Hebling, J.; Almasi, G.; Kozma, I.; Kuhl, J. Velocity Matching by Pulse Front Tilting for Large Area THz-pulse Generation. *Opt. Express* **2002**, *10*, 1161−1166.
(26) Planken, P. C. M.; Nienhuys, H.-K.; Bakker, H. J.; Wenckebach, T. Measurement and Calculation of the Orientation Dependence of Terahertz Pulse Detection in ZnTe. *J. Opt. Soc. Am. B* **2001**, *18*, 313−317.
(27) van der Valk, N. C. J.; Wenckebach, T.; Planken, P. C. M. Full Mathematical Description of Electro-Optic Detection in Optically Isotropic Crystals. *J. Opt. Soc. Am. B* **2004**, *21*, 622−631.
(28) Fang, T.; Konar, A.; Xing, H.; Jena, D. Carrier Statistics and Quantum Capacitance of Graphene Sheets and Ribbons. *Appl. Phys. Lett.* **2007**, *91*, 092109-1−092109-3.
(29) Ferrari, A. C.; Meyer, J. C.; Scardaci, V.; Casiraghi, C.; Lazzeri, M.; Mauri, F.; Piscanec, S.; Jiang, D.; Novoselov, K. S.; Roth, S.; Geim, A. K. Raman Spectrum of Graphene and Graphene Layers. *Phys. Rev. Lett.* **2006**, *97*, 187401-1−187401-4.
(30) Rana, F. Electron-hole generation and recombination rates for Coulomb scattering in graphene. *Phys. Rev. B* **2007**, *76*, 155431-1−155431-5.
(31) Winzer, T.; Knorr, A.; Malic, E. Carrier Multiplication in Graphene. *Nano Lett.* **2010**, *10*, 4839−4843.
(32) Winnerl, S.; Göttfert, F.; Mittendorff, M.; Schneider, H.; Helm, M.; Winzer, T.; Malic, E.; Knorr, A.; Orlita, M.; Potemski, M.; Sprinkle, M.; Berger, C.; d. Heer, W. A. Time-resolved spectroscopy on epitaxial graphene in the infrared spectral range: relaxation dynamics and saturation behavior. *J. Phys.: Condens. Matter* **2013**, *25*, 054202-1−054202-14.